Applied Surface Science 447 (2018) 107–116

Contents lists available at ScienceDirect

Applied Surface Science

journal homepage: www.elsevier.com/locate/apsusc

Full Length Article

# Novel NiFe/NiFe-LDH composites as competitive catalysts for clean energy purposes

A.M.P. Sakita [a,b], E. Vallés [b,c], R. Della Noce [d,e], A.V. Benedetti [a,*]

[a] São Paulo State University, Institute of Chemistry, 55 Prof. Francisco Degni St., 14800-060 Araraquara, São Paulo, Brazil
[b] Ge-CPN (Thin Films and Nanostructures Electrodeposition Group), Dpt. Ciència de Materials i Química Física, Martí i Franquès 1, 08028 Barcelona, Spain
[c] Institute of Nanocience and Nanotechnology (IN2UB), Universitat de Barcelona, Spain
[d] Faculdade de Química, Instituto de Ciências Exatas e Naturais, Universidade Federal do Pará, Rua Augusto Corrêa, 1, 66075-110 Belém, PA, Brazil
[e] Centro de Química Estrutural-CQE, Departament of Chemical Engineering, Instituto Superior Técnico, Universidade de Lisboa, 1049-001 Lisboa, Portugal

ARTICLE INFO

*Article history:*
Received 24 January 2018
Revised 23 March 2018
Accepted 28 March 2018
Available online 29 March 2018

*Keywords:*
Electrodeposition
Byproducts
Ni-Fe LDH
Oxygen evolution reaction

ABSTRACT

The electrodeposition of metals generally employs several additives to avoid the formation of undesirable byproducts such as oxides and hydroxides. Although the deposition of metals is still the main goal in the most metals electroplating, the applicability of these byproducts might be an interesting field which is not explored in detail so far. In this work, the significance of water splitting reaction in clean energy production, employing NiFe hydroxides formed during the metals electrodeposition, is demonstrated for oxygen evolution reaction. The synthetized materials are composites of three components easily prepared in one-step by means of electrodeposition. Specifically, a granular NiFe alloy is obtained over which local pH variation and chloride presence induce the formation of a layered double hydroxide structure. The study of the influence of solution composition, deposition time, and deposition potential on the catalytic properties of the composites with respect to the oxygen evolution reaction are analyzed. Deposition times of few seconds, deposition potentials in the range −1.4 to −1.6 V vs. Ag/AgCl/KCl3M, and solutions containing Fe(II), Ni(II) and high chloride concentrations, lead to the best catalysts, showing an $\eta_{10\ mA\ cm-2}$ about 0.280 V.



## 1. Introduction

Metal oxy/hydroxides have received great attention as materials suitable for many applications mainly as anode for water splitting (WS) cells, a fundamental device in the field of energy conversion and storage [1–4]. The search of new materials and methods for storing renewable energy is primordial to replace fossil fuels; a great challenge in the current world. Hydrogen is a fundamental chemical resource for clean energy generation due to its high energy density, which guarantees the applicability by means of burning it or in fuel cells. However, to be applicable in fuel cells, it is needed a highly pure hydrogen [5] but currently hydrogen is obtained by the steam-reforming of fossil fuels, which generates $CO_2$ as one of the products of the reaction. As an alternative, the WS is a technology of no $CO_2$ emission [6]. On other hand, the WS requires the improvement of both efficiency and costs of production. For example, the utilization of noble metals as electrodes implies a good efficiency of the WS process [7,8] with low overpotentials for both hydrogen evolution reaction (HER) and oxygen evolution reaction (OER) [9], but the cost of producing these electrodes is too high because the precursors are very expensive, and the large-scale applicability of these materials is difficult. As an alternative to reduce the costs for WS process, new procedures for easily fabrication and the development of new catalysts based on oxy/hydroxides of earth-abundant metals have been proposed since they have shown promising results for OER. Qi et al. [10] have demonstrated that nickel-iron oxides exhibit, for this reaction, overpotentials about 330 mV to reach current densities of 10 mA $cm^{-2}$ in alkaline solution (0.1 M KOH). Cobalt-iron oxides have been also studied for WS, and CoFe oxides synthetized by chemical reduction using borohydrate-nitrate medium have showed overpotentials lower than those obtained using rare metals oxides such as $RuO_2$ [11]; nevertheless, CoFe oxy/hydroxides display worse catalytic properties when compared to NiFe ones, a fact that is positive owing to the lower price of nickel.

The preparation method of OER catalysts is fundamental to successively implement them at industrial level. Solvothermal [12–14] and hydrothermal [15–17] synthetic routes have been proposed to produce nanostructured materials appropriate for

* Corresponding author.
*E-mail address:* benedeti@iq.unesp.br (A.V. Benedetti).

https://doi.org/10.1016/j.apsusc.2018.03.235
0169-4332/

OER catalyst but they are expensive methods that imply long time of synthesis, further cleaning and separation of the catalysts, and high temperatures. Furthermore, the catalysts must be incorporated on the electrode by means of binders. Electrodeposition can be an alternative and low cost method for OER catalysts fabrication because it allows room-temperature and large-scale fabrication and, moreover, permits the synthesis directly on the electrode avoiding the use of binders [18–22]. In this line, electrochemical fabrication of NiFe oxy/hydroxides and layered double hydroxides (LDH) structures as catalysts for OER have been proposed, through assisted electroreduction of $NO_3^-$ (Eq. (1)), which induces the formation of $OH^-$ ions promoting the hydroxides precipitation on the surface electrode [23,24] (Eq. (2)):

$$NO_3^- + 7H_2O + 8e^- \rightarrow NH_4^+ + 10OH^- \quad (1)$$

$$M^{n+} + xOH^- \rightarrow M_xOH_n \quad (2)$$

Another approach to prepare these catalysts is the electrodeposition of NiFe films and posterior oxidation in alkaline medium to obtain catalytic oxides [25,26], which exhibits good catalytic responses but makes the process laborious. Oxides and hydroxides formation is usually prevented in metals or alloys electrodeposition [27–29], but it might be interesting for the synthesis of oxidized species for water splitting. In this context, we have recently proposed a nitrate-free, one-step and fast electrodeposition process to obtain films of CoFe covered with LDH [18] that may be adequate to catalyze OER reaction. Recently, the chemical deposition of iron oxidized species onto nickel foam (NF) was reported where it was demonstrated that after a further oxidation in alkaline medium, a layered double hydroxide structure were formed in the NF surface [30]. Although the proposed method reveals to be scalable and fast for the synthesis of catalysts, the difference between the $\eta_{10\ mA\ cm-2}$ value of bare NF and NiFe-LDH/NF does not shows significant values (higher than 100 mV) as compared to other works [17,18,31,32].

Herein, we present a novel electrochemical procedure to prepare competitive catalysts (glassy carbon/NiFe alloy/NiFe-LDH composites) for OER, exhibiting the following advantages: (1) it is a fast (few seconds), easy and one-step method to obtain, without the use of binders, stable catalysts, (2) directly allows obtaining both a conductive sub-layer of NiFe alloy of high surface area and the catalytic NiFe-LDH open structure containing chloride ions, (3) does not require the use of nitrate, (4) permits the formation of catalysts of defined area and (5) uses a simple deposition bath. Additionally, this work shows the utilization of so-called byproducts in metal electrodeposition and analyzes the influence of each one of the factors controlling the deposition procedure (time-deposition, bath composition and applied potential) to optimize the conditions for obtaining the more effective composites for OER. A simple way to evaluate the potentiality of the electrodeposits by a simple voltammetry scan of the deposition bath is also demonstrated.

## 2. Experimental details

### 2.1. Electrodeposition process and catalyst synthesis

The deposition bath was prepared by dissolving $FeCl_2.4H_2O$ (Sigma-Aldrich 99.0%) and $NiCl_2{\cdot}6H_2O$ (Panreac Analytical Grade) in Milli-Q quality water. Different amounts of KCl were added to analyze the influence of the chloride concentration in the deposition process and in the characteristics of the deposits. The solution was purged and maintained in Ar atmosphere, to avoid the $Fe^{2+}$ oxidation during all the deposition process. The pH of the solution varied from 2.5 to 4, depending on the salts concentration.

Glassy carbon (GC) electrodes with geometric area of 0.071 $cm^2$ were polished to mirror-like finishing with alumina slurry of 0.3 μm and employed as working electrodes. For the electrodeposition process, an $Ag|AgCl|KCl_{(3M)}$ reference electrode was used, while the counter electrode was a Ti/Rh spiral.

The deposits were prepared potentiostatically by using a microcomputer-controlled potentiostat/galvanostat AUTOLAB PGSTAT30 and the GPES software. The potentials were applied for different times from 1 to 60 s for all the deposited materials.

### 2.2. Electrochemical response of the catalyst

Polarization curves of the deposits prepared on GC were recorded at a scan rate of 5 mV $s^{-1}$ in 1 M NaOH solution, using a reversible hydrogen electrode (RHE) as reference electrode and a Ti/Rh spiral as counter electrode. Electrochemical surface area (ECSA) was obtained in NaOH 1 M at 50 mV about the region of double layer capacity (region without Faradaic contribuition) in different scan rates.

### 2.3. Surface characterization

The prepared materials were characterized by XPS (X-ray photoelectron spectroscopy), with a PHI 5500 Multitechnique System (from Physical Electronics) containing a monochromatic X-ray source (Aluminium Kalfa line of 1486.6 eV energy and 350 W). X-ray diffracttometry (XRD) was performed with a PANalytical X'Pert PRO MPD powder diffractometer, with Bragg–Brentano geometry and θ/θ goniometer. Nickel filtered Cu Kα radiation (λ = 1.5418 Å) and a work power of 45 kV–40 mA were used. Field emission scanning electron microscopy (FE-SEM) analysis was performed using a JEOL J-7100 operating with electron acceleration of 2 keV.

## 3. Results and discussion

### 3.1. Study of Ni-Fe electrodeposition

Voltammetric studies of the Ni(II) + Fe(II) system in acidic chloride medium have been performed over glassy carbon (GC) substrates to define the influence of chloride concentration and [Ni(II)]/[Fe(II)] ratio on the deposition bath. The electrodeposition process of the Ni-Fe system has been studied at different [Ni(II)]/[Fe(II)] ratios (1/0.25 to 1/1) and compared with the electrodeposition of both pure Ni and Fe in the same medium (Fig. 1). In all cases, the voltammetric curves of the Ni-Fe system allow to detect, in the cathodic scan, a small current, corresponding to proton reduction [33,34], followed by a clear reduction peak due to Ni-Fe deposition and, at more negative potentials [34], a new reduction current related to massive hydrogen evolution (Fig. 1A–C). The exact position and intensity of the deposition peak is obviously dependent on the specific concentrations. The comparison of the voltammetric curves with those of pure-Ni (Fig. 1D) and pure-Fe (Fig. 1E) demonstrates that Ni and Fe deposit simultaneously (in a single peak) in the Ni-Fe solution. Deposits were more easily oxidized when the iron content (the less noble metal) in the Ni-Fe deposits increased, revealing that Ni-rich alloys are more resistant to the oxidation. The increasing on $[Ni^{2+}]$ decreases the oxidization due to the fast formation of a passive layer based on nickel species, which block the surface and prevent the electro-oxidation of the alloy. In nickel and nickel-iron electrodeposition the addition of boric acid on the plating bath are common to avoid the surface passivation [35], however, in this work, the absence of additives are desirable to improve the byproducts formation.

Chloride ions form complexes with the cations (although in low proportion) (Fig. 2 [36]) and also can adsorb on the electrode or in

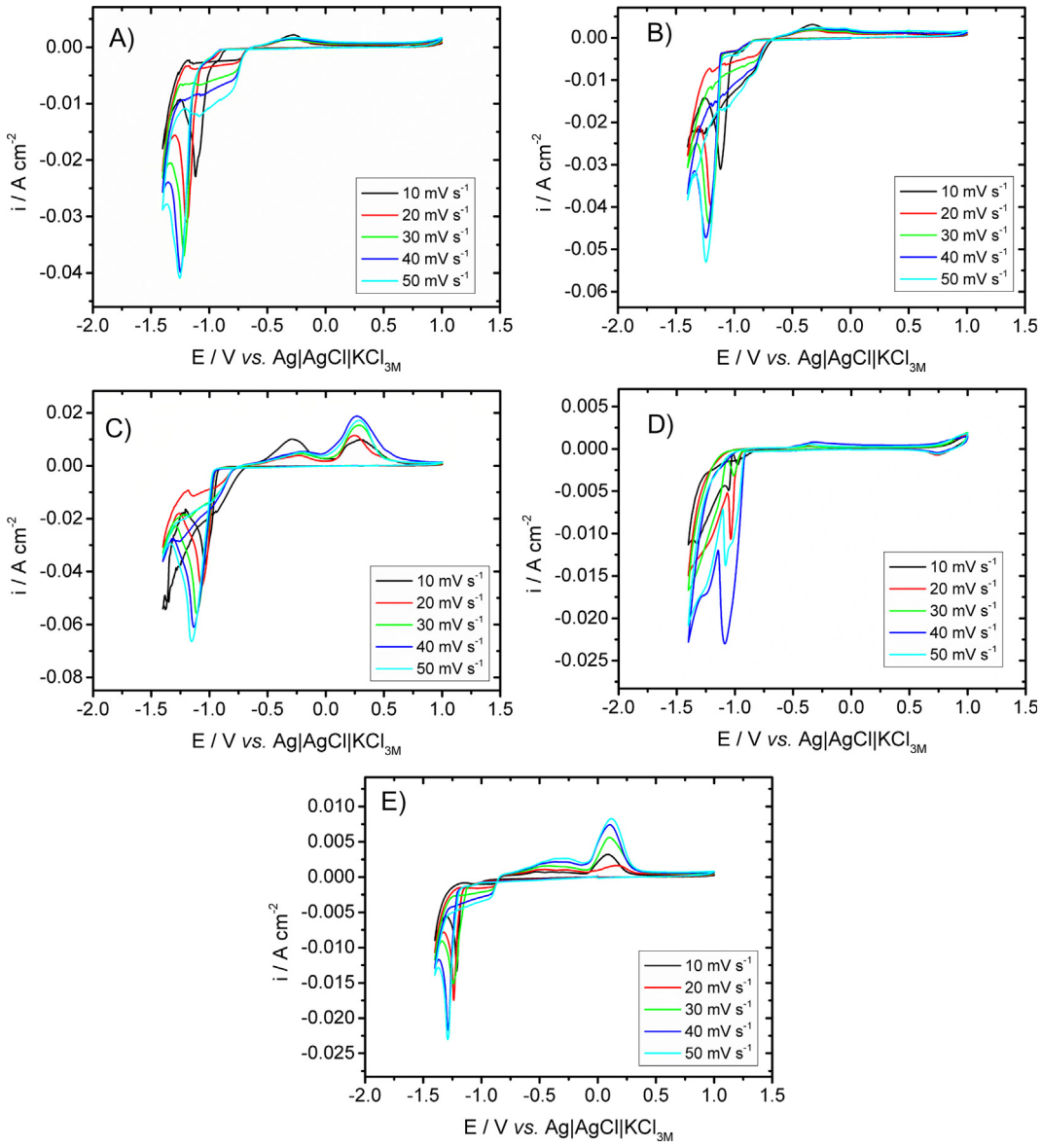


**Fig. 1.** Cyclic voltammetry of the deposition baths of (A) NiFe 0.1:0.025 M, (B) NiFe 0.1:0.05 M, (C) NiFe 0.1:0.1 M, (D) Ni 0.1 M, and (E) Fe 0.05 M.

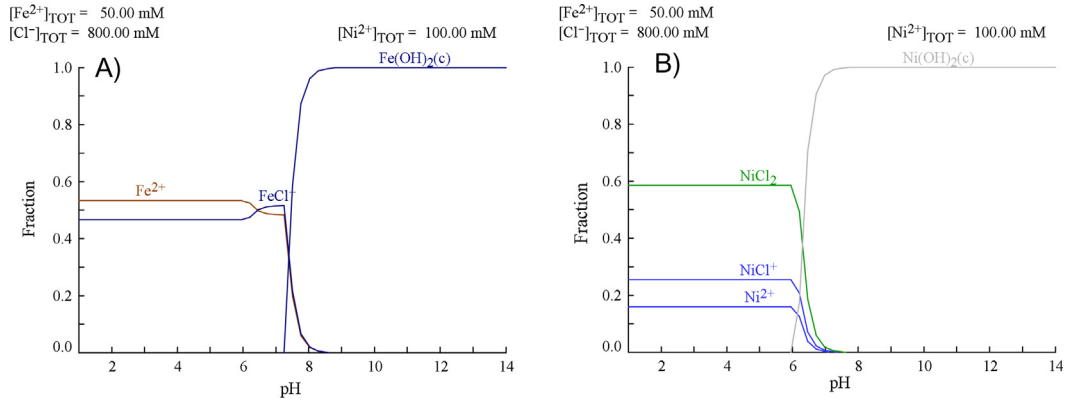


**Fig. 2.** Fraction of different (A) $Fe^{2+}$ and (B) $Ni^{2+}$ species as a function of the pH in an aqueous chloride-containing system [36].

the deposit [37,38], as the manner that the deposition process can be affected by the chloride concentration. Fig. 3A and B shows that when potassium chloride is added to the Ni-Fe solution (Fig. 3A), the reduction current in the backward scan clearly decreases because of the adsorption of free chloride ions on the initial formed deposit. In the anodic scan, oxidation current drastically decreases

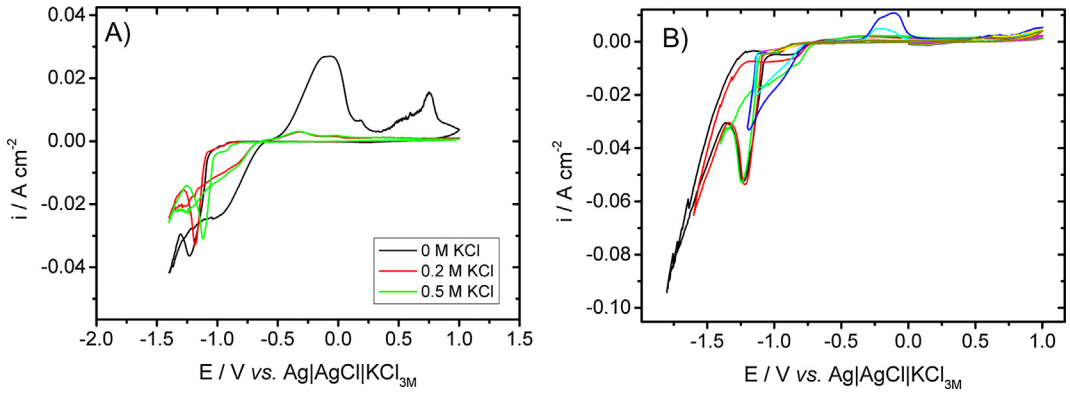


**Fig. 3.** Cyclic voltammograms of a $FeCl_2$ 0.05 M + $NiCl_2$ 0.1 M, (A) at 10 mV $s^{-1}$, with different chloride concentrations and (B) at 50 mV $s^{-1}$ with KCl 0.5 M at different inversion potentials.

as the chloride concentration increases, which reveals a higher stability of the deposits prepared in an excess of chloride. Therefore, 0.5 M has been selected as the more adequate concentration of KCl. Moreover, a high concentration of chloride ions is desired to favor the entrapment of these ions during the forced formation of oxidized species during the electrodeposition, in order to form NiFe-LDH structures.

When, in this solution, different cathodic limits can be compared (Fig. 3B); it is observed that when the cathodic limit attains the potentials corresponding to hydrogen evolution, oxidation of the deposits clearly decreases, which discloses the formation of oxidized species over the initial Ni-Fe that hinders (passivates) alloy oxidation. Metal hydroxides were formed over the metallic deposit because of the local variation of pH on the electrode accompanying hydrogen evolution.

### 3.2. Preparation and characterization of NiFe-based catalysts

Voltammetric studies have been carried out to select different potentials to perform the synthesis of Ni-Fe-based catalysts for OER, one corresponding to the onset of the deposition process (−1.0 V), other related to metals deposition followed by some hydrogen evolution (−1.4 V), and the third regarding the massive hydrogen evolution over metallic deposit formation (−1.8 V). Fig. 4 shows the shape of the chronoamperometric curves recorded during fast deposits formation. The curves display that when the potential is more negative, a second process takes place, after the reduction of the metallic ions. This second process corresponds to hydrogen evolution, very significant at −1.8 V, as the manner that at −1.4 and −1.8 V the formation of oxidized species is expected over the first deposited metals, as a consequence of the local pH variation accompanying the hydrogen gas formation. When the deposits are observed by SEM, a thin layer of granular deposit is detected by applying −1.0 V, whereas at −1.4 V the deposit shows, over the metallic thin layer, a non-compact layer, probably of oxidized species. Deposits obtained at −1.8 V are mostly composed of the oxidized species. The mechanism of hydroxide growth in chloride medium was evaluated in a recent work of Ritzert and Moffat [39] by the study of $Ni(OH)_2$ formation during the electrodeposition of metallic Ni on gold microelectrode. The authors showed by *in situ* microscopy and cyclic voltammetry employing SECM (scanning electrochemical microscopy) that under potentials higher than −1.5 V, the hydroxides products were deposited heterogeneously upon the surface, while at lower deposition potentials, the fast nucleation of $Ni(OH)_2$ induces the homogeneous deposition. This fact agrees with the morphologies obtained in this work.

All the deposits present oxygen and chlorine in their structure (Table 1, EDS results), but with an increasing proportion of both components as the deposition potential is shifted to more negative values. The fast deposition rate at negative potentials and the oxidized layer formation can favor the entrapment of chloride ions in the global deposited structure. The Ni:Fe ratio in the deposits varied from 3:1 to 2:1 in the −1.0 to −1.8 V potential range since the voltammetric curve reveals that nickel electrodeposition (Fig. 1D) starts at less negative potentials than iron (Fig. 1E) leading to Ni richer deposits at −1 V. On the other hand, the standard reduction potential for $Ni^{2+}$ is nobler than $Fe^{2+}$ and the increase on Ni content on the deposit obtained at −1.0 V is consistent. The present composition used in this work reveals that there is no anomalous codeposition in the NiFe alloys, as expected for a high chloride concentration solution [40].

The high resolution (HR) XPS spectra of the different elements show (Fig. 5) that the chemical environment of all the elements is very similar, except for oxygen. The Ni 2p peaks at 855.8 and 873.5 eV, associated to the Ni $2p_{3/2}$ and Ni $2p_{1/2}$ bands of Ni-OH bonds, and the satellite peaks at 861.5 and 879.3 eV, exhibit the presence of nickel(II) hydroxides [41]. The deposit obtained at −1.8 V shows a small peak at 852.7 eV related to the Ni $2p_{3/2}$ of a metallic phase, and a small band at 706.7 of Fe(0), indicating a NiFe alloy. Nevertheless, these peaks are not observed in the deposit obtained at −1.4 V, probably due to the presence of a thicker oxide layer. The bands at 711.3 and 725.0 eV are related to the binding energy of Fe $2p_{3/2}$ and Fe $2p_{1/2}$ in Fe(III) environment [42,43]. Li et al. [44] reported similar XPS data for NiFe-LDH electrodeposited in nitrate solution, where only hydroxylated species were synthetized . The Ni 2p and Fe 2p signals indicate that the samples prepared at −1.4 and −1.8 V present similar oxidized species on the surface of the deposit, mainly of Ni(II) and Fe(III), but the higher thickness of the LDH obtained at −1.4 V does not permit the detection of the metallic layer. The similar Ni and Fe species in the HR-XPS spectra of the two samples are also observed in the Cl 2p band. The Fig. 5C (HR-XPS Cl 2p) shows two peaks at 198.0 and 199.5 eV, with a $\Delta E_B$ (Difference between $2p_{1/2}$ and $2p_{3/2}$ peaks) of 1.6 eV, corresponding to the Cl $2p_{3/2}$ and Cl $2p_{1/2}$ to a chlorine in ionic state [45], which indicates that chloride species are inside the metal oxide matrix, as expected for a chlorine LDH interlayer. The O 1s spectrum depicts contributions at 529.7, 531.4 and 532.6 eV on the spectra of the −1.8 V deposit (see deconvoluted spectra at supporting information), which can be assigned to metal-oxygen, M–O–H, oxygen ions at the surface with low coordination [46] and structural water bonded and inside the deposit structure [47], respectively. All the deconvoluted HR-XPS spectra can be seen in Fig. S1.

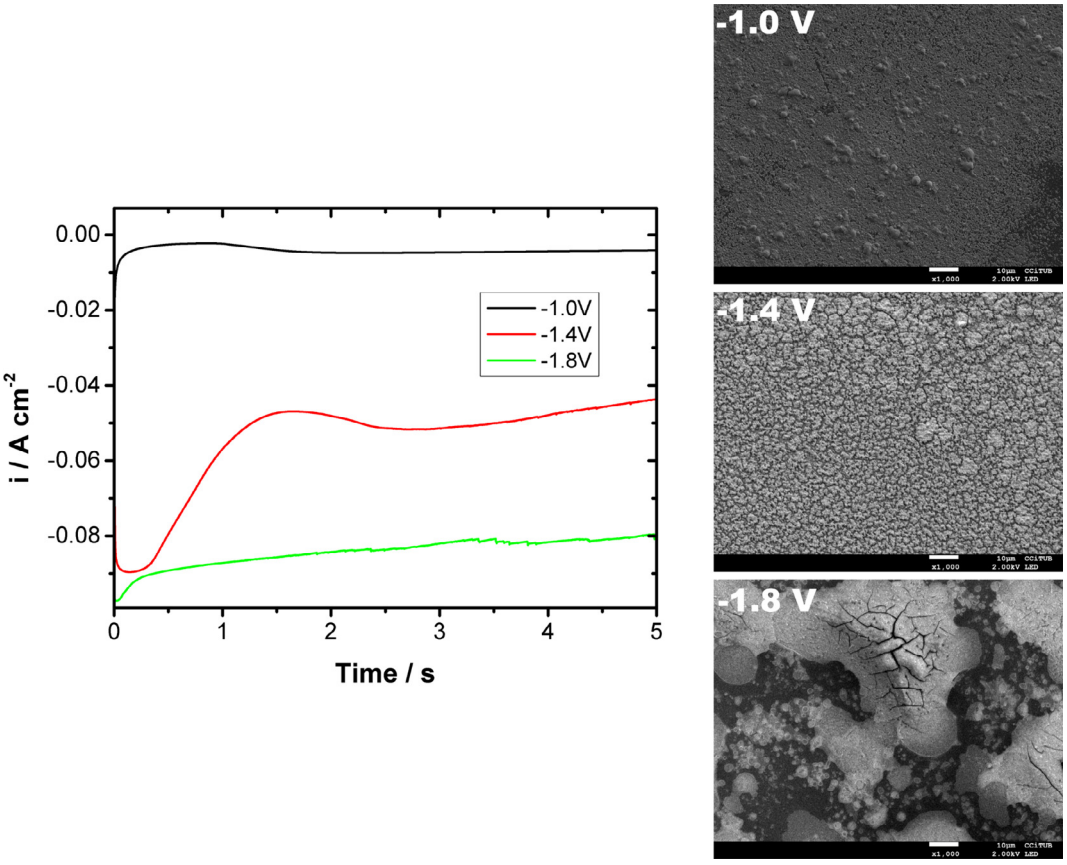


**Fig. 4.** Chronoamperometric curves and SEM images of the deposits obtained at different potentials.

**Table 1**
Deposits composition obtained by EDS.

| Deposition Potential/V | Ni/at.% | Fe/at.% | O/at.% | Cl/at.% |
|---|---|---|---|---|
| −1.0 | 39.0 | 12.8 | 44.8 | 3.4 |
| −1.4 | 15.6 | 6.3 | 69.0 | 9.1 |
| −1.8 | 15.9 | 7.9 | 57.7 | 18.5 |

The XRD profiles of the deposits obtained at −1.0 and −1.4 V are illustrated in Fig. 6. In both cases, a crystalline fcc metallic phase of Ni-Fe alloy (Ni-rich) is formed (PDF-65-3244 pattern), corresponding to a Ni-Fe with Ni-rich phase [48], which agrees with the composition obtained by EDS and with the [Ni(II)]/[Fe(II)] ratio in the solution. Deposit obtained at −1.4 V presents diffraction peaks of both Ni-Fe alloy (in red) [49,50] and NiFe-LDH structure (in blue) [51], which corroborates the oxidized species also observed by XPS. The crystalline grain size for the Ni-Fe alloy has been estimated by Scherrer's method and reveals to be 23 nm and 15 nm for the deposits obtained at −1.0 and −1.4 V, respectively. The large peaks of the NiFe-LDH (in blue) ca. 34° and 61° 2θ degrees are observed due to the overlap of two peaks and can be attributed to the nanocrystalline behavior of the LDH products. The observed metallic alloy on the XRD pattern of the sample obtained at −1.4 V agrees with the metallic nanograins showed by SEM (Fig. 4).

As a summary of the characterization of the deposits obtained from the selected bath, we found that, through a simple one-step procedure, deposits are constituted of a granular Ni-Fe alloy covered by Ni(II) and Fe(III) oxidized species, identified as NiFe-LDH structures (containing chloride), which might be promising effective and stable catalysts for OER in alkaline medium. The scheme showed in Fig. S2 represents the multi-layered structure obtained at −1.4 V, composed of Ni-Fe nanoparticulate alloy covered with NiFe-LDH, with water and chlorine in its interlayer structure and Fig. S3 demonstrates the steps involved in the multilayered composite growth.

### 3.3. Test and optimization of catalysts for OER

The GC/NiFe/NiFe-LDH structures have been tested as effective catalysts for OER in alkaline medium. Deposits prepared at different potentials, chloride concentrations and [Ni(II)]/[Fe(II)] ratios have been used to enhance the oxygen evolution reaction, in order to select the best catalysts, based on the quantification of the onset potential, overpotential, and Tafel slope for the reaction. The influence of the deposition potential on the catalytic properties of the films is shown in Fig. 7A and Table 2, which suggests best catalytic properties at more negative applied potentials for the deposition. However, by the chronopotentiometric curves (Fig. 7B) obtained at 10 mA $cm^{-2}$ (in geometric area) is possible to observe lower overpotentials when the deposition potentials are ca. −1.3 to −1.6 V. This behavior is owing to the observation of different surface reactions at 10 mA $cm^{-2}$ in the polarization curves, instead of OER. At deposition potentials lower than −1.3 V, it is observed two small shoulders on the polarization curves (ca. 10 mA $cm^{-2}$), attributed to a residual current of the Ni(II) to Ni(III) oxidation in the Ni-rich alloy (less positive potentials) [52] followed by the Ni (II) to Ni(III) reaction on the NiFe-LDH [53]. In this sense, the obtaining overpotential by the chronoamperometric curves is more reliable and reveals lower $\eta_{10mA\ cm-2}$ for the materials prepared at −1.4 V. To comprehend the high catalytic performance obtained at −1.4 V, electrochemical active surface science of the materials deposited in different potentials were obtained from the cyclic voltammetry of the double layer zone (Fig. S3). Deposits

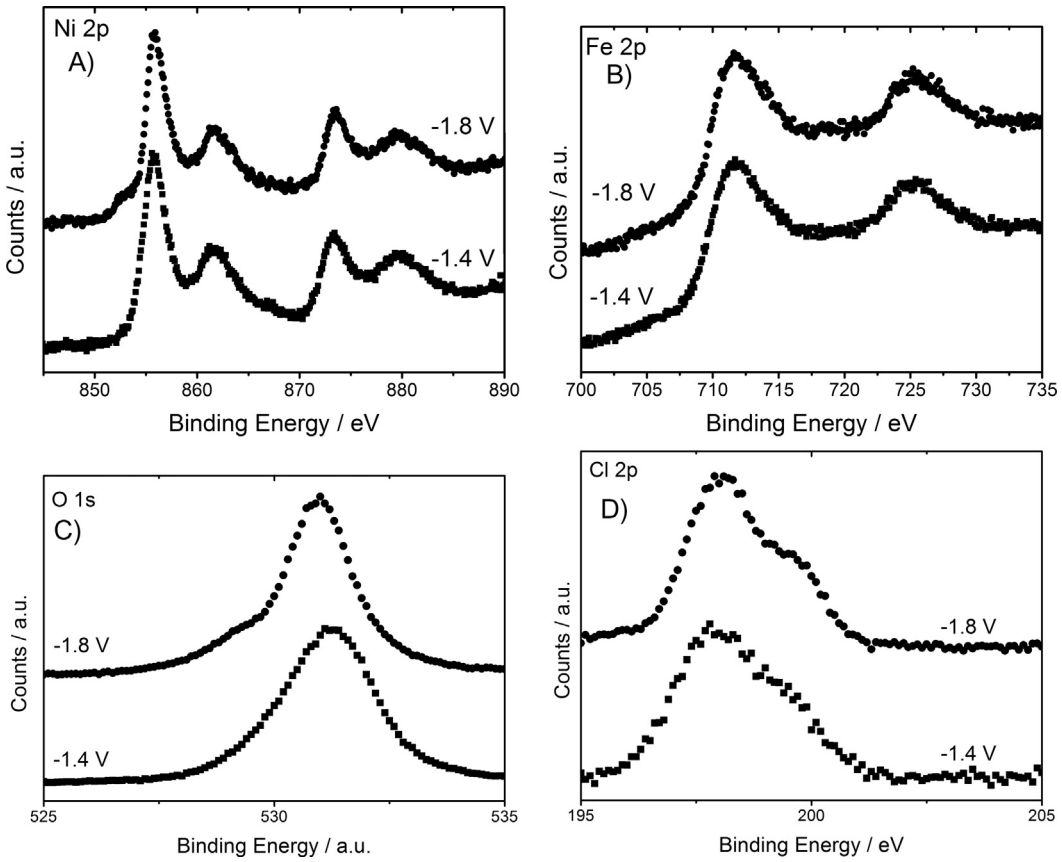


**Fig. 5.** XPS-HR (a) Ni 2p, (b) Fe 2p, (c) O 1s and (d) Cl 2p of the deposit obtained at −1.4 and −1.8 V *vs* Ag|AgCl|$KCl_{3M}$ during 5 s.

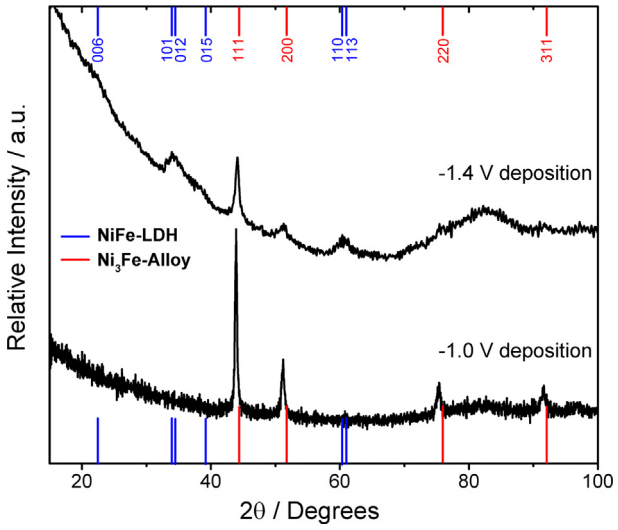


**Fig. 6.** XRD patterns of deposits obtained at −1.4 and −1.0 V *vs.* Ag|AgCl|KCl(3M). Blue pattern: NiFe//LDH, red pattern: $Ni_3Fe$ alloy.

prepared at −1.4 V present the maximum value of $C_{DL}$ (double layer capacitance), which suggests a higher electrochemical surface area (ECSA) for these deposits, in according to their best catalytic performance. ECSA values clearly decrease for the deposits prepared at potentials more negative than −1.6 V, probably due to the formation of a very thin layer of LDH as it is observed by XPS when the metallic sub-layer is detected.

At the best conditions (−1.4 V, 1:0.5 Ni: Fe ratio, [KCl] = 0.5 M and deposition time of 5 s) Tafel slopes were about 120 mV $dec^{-1}$, which suggests that the third step of the OER reaction is the rate determinant one [54]. In general, Tafel slopes increase when the Ni:Fe ratio also increases, which demonstrates that the incorporation of Fe into the Ni deposits improves the catalytic performance (Table 2). Furthermore, IR drop correction has not been applied to the curves showed in Fig. 7, which may cause an overestimation of $\eta_{10\ mA\ cm-2}$ and Tafel slopes. Although the modernity of the instruments allow a real time correction by positive feedback and current interrupt IR compensation, a careful attention should be attained because the over correction of the IR drop decreases the values of Tafel Slope and overpotential, leading to misleading results.

The deposition time has been also optimized by analyzing the polarization curves of the deposited catalysts (Fig. 8A). Too short times of synthesis (1 s) lead to high $\eta_{10mAcm-2}$, due to the formation of deposits mainly constituted by metallic Ni-Fe alloy. On the other hand, deposition times higher than 5 s lead to deposits with excessive proportion of hydroxides, as can be deduced by the higher deposition time, or with lower catalytic sites. Therefore, the best catalytic properties are obtained for deposits prepared in the interval of 1–10 s. With regard to the influence of the chloride concentration (Fig. 8B), the catalytic properties improve when the concentration is high, indicating that chloride interlayer enhances the OER catalysis. Recently, Kou et al. [55] studied the doping of Co $(OH)_2$ with chlorine for OER, and showed that Cl-doped $Co(OH)_2$ exhibits better performance for OER than the non-doped material. The main explanation given by the authors is the introduction of defects in the materials, which develops new active sites for the oxidative catalysis. Lastly, increasing the [Ni]/[Fe] ratio from 1 to 4, the $\eta_{10\ mA\ cm-2}$ decreases revealing the importance to attain the Fe-sites on the NiFe-LDH. The best catalytic performance for

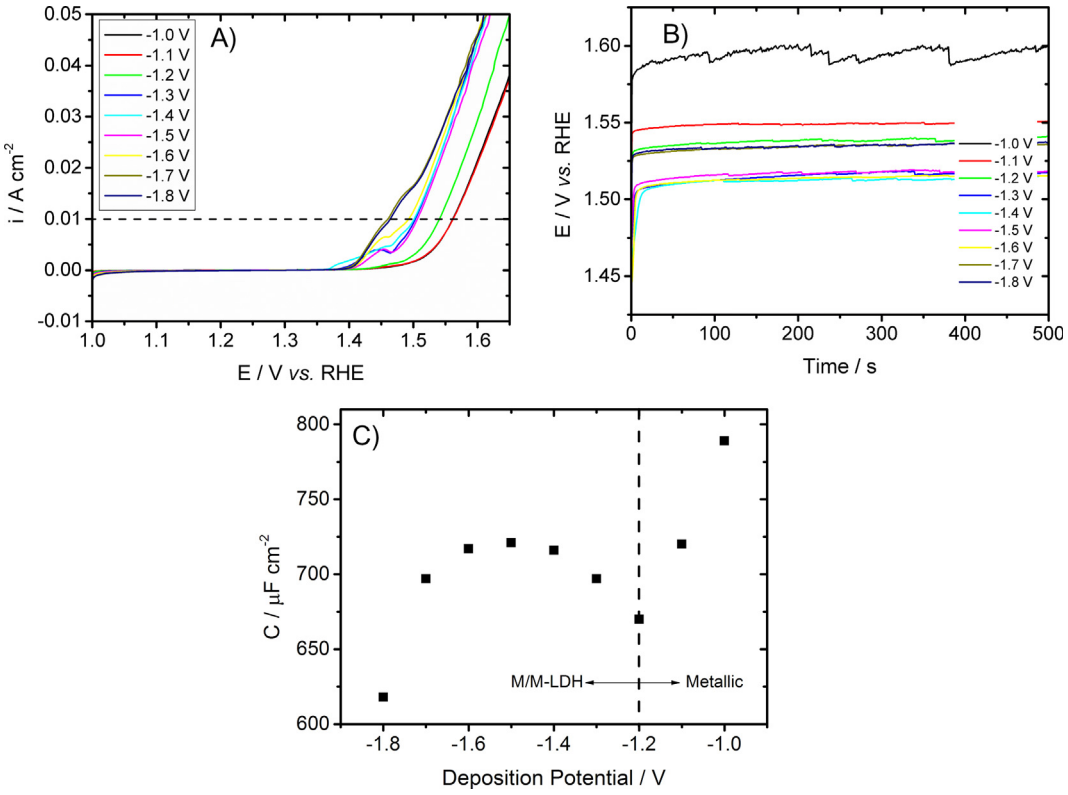


**Fig. 7.** (A) Polarization curves obtained at 5 mV $s^{-1}$, (B) Chronopotentiometric curves for deposits obtained at different potentials in 1 M NaOH solution and (C) $C_{dl}$ of the materials deposited at different potentials.

**Table 2**
Catalytic parameters of the different conditions of electrodeposition. PC is for the parameters obtained polarization curves and CP for chronopotentiometric.

| Deposition Potential/V | Time/s | KCl in solution/M | Ni:Fe | PC$\eta_{onset}$/V | PC$\eta_{10\ mA\ cm-2}$/V | Tafel Slope/mV $dec^{-1}$ | CP$\eta_{10\ mA\ cm-2}$/V |
|---|---|---|---|---|---|---|---|
| −1.0 | 5 | 0.5 | 1:0.5 | 0.294 | 0.332 | 83 | 363 |
| −1.1 | | | | 0.294 | 0.332 | 79 | 320 |
| −1.2 | | | | 0.275 | 0.311 | 79 | 310 |
| −1.3 | | | | 0.247 | 0.273 | 102 | 287 |
| −1.4 | 1 | 0.5 | 1:0.5 | 0.269 | 0.310 | 84 | – |
| | 5 | 0 | 1:0.5 | 0.290 | 0.342 | 97 | – |
| | | 0.2 | 1:0.5 | 0.238 | 0.282 | 127 | – |
| | | 0.5 | 0:0.5 | 0.380 | >450 | 168 | – |
| | | | 1:1 | 0.272 | 0.320 | 107 | – |
| | | | 1:0.5 | 0.242 | 0.271 | 112 | 284 |
| | | | 1:0.25 | 0.245 | 0.274 | 120 | |
| | | | 1:0 | 0.280 | >450 | 228 | |
| | 10 | 0.5 | 1:0.5 | 0.257 | 0.292 | 126 | |
| | 20 | 0.5 | 1:0.5 | 0.266 | 0.298 | 151 | |
| −1.5 | 5 | 0.5 | 1:0.5 | 0.245 | 0.277 | 81 | 289 |
| −1.6 | | | | 0.238 | 0.263 | 124 | 286 |
| −1.7 | | | | 0.221 | 0.230 | 210 | 306 |
| −1.8 | | | | 0.222 | 0.235 | 202 | 306 |

the OER is reached when the deposits are obtained in conditions that passivated species are formed and detected in the stripping scan of the voltammetric curves (Figs. 1 and 3). In addition, better performance is also achieved with low $Fe^{2+}$ concentration in the solution, because an increase of its concentration leads to lower amount of hydroxylated species in the deposit. The nature of catalytic properties have been reported to iron(III) octahedral sites on the $NiO_xH_y$ surface [56] inducing edges/defects, which promotes a slightly decrease of the $e^-$ per nickel and the conductivity [57]. Differently from the approach showed by Klaus et al. [58], in this work the impurities of the electrolyte by iron ions should not influence the response of the catalyst due to the direct synthesis of the mixed oxy/hydroxide by electrodeposition. Although the similar response of catalyst prepared by electrodeposition and sputtering as studied by Bell group [59], the methodology employed for the present study reveals an deposition of metal/hydroxides composites and furthermore allows the intercalation by chloride ions, which displays better results for OER than the typical $NO_3^-$ intercalated anions [51].

The correlation found between the quality of the catalysts in the polarization curves of OER and the cyclic voltammetric response of the deposition baths allows proposing a novel and simple way to

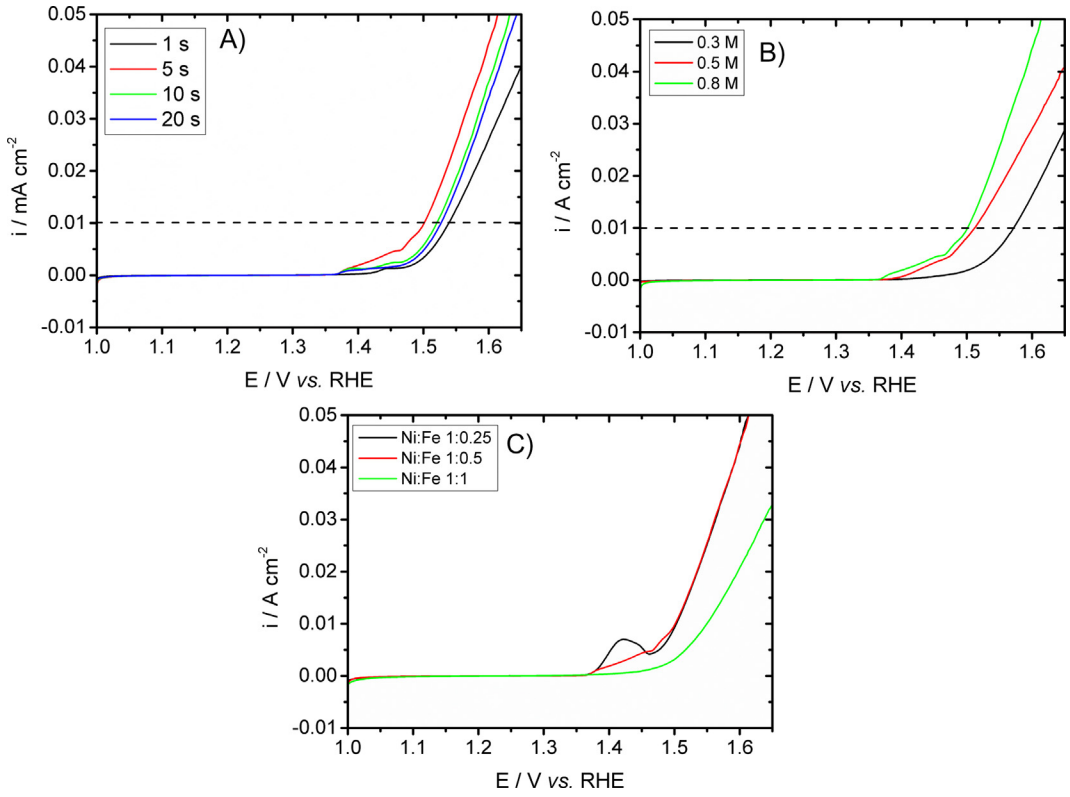


**Fig. 8.** Polarization curves for deposits obtained at 5 mV $s^{-1}$ at different (A) deposition time. (B) chloride concentration and (C) Ni:Fe ratios.

evaluate transition metal oxides/hydroxides as promising OER electrocatalysts.

Once optimized the best catalysts for OER from the results of Table 2, the comparison with previous catalysts proposed in the literature (Table SM1 of supplementary material) reveals that not only the procedure of preparation is easier and faster, but also the GC/Ni-Fe/NiFe-LDH composites are really new competitive materials for OER.

## 4. Conclusion

The utilization of typical byproducts formed during metals electrodeposition for catalytic purpose has been demonstrated and the best conditions for their synthesis evaluated. By employing a one-step ultra-fast electrodeposition (few seconds) in a free-nitrate Fe (II) + Ni(II) solution on glassy carbon substrate permits directly obtain effective hydroxides layers upon a metallic matrix. The best conditions (−1.4 V, 5 s) are those leading to the formation of a conductive granular Ni-Fe layer over which a non-compact LDH layer with intercalated chloride has been formed. Moreover, the best catalysts must include chloride intercalated in the LDH. The easy method and the excellent catalyst properties ($\eta_{10\ mA\ cm-2} \sim 280$ mV, Tafel slopes <120 mV $dec^{-1}$) show that our procedure and material are efficient and is an alternative to the current procedures for the synthesis of OER catalysts.

## Acknowledgment

The authors thank the Brazilian funding CAPES (proc. no. 88881.132671/2016-01) and CNPq (proc. no. 141257/2014-8), Portuguese FCT Funding Agency (project PEst-OE/QUI/UI0100/2013), EU ERDF (FEDER) and the Spanish Government grants (TEC2014-51940-C2-R). The authors thank the CCiT-UB for the use of their equipment.

## Appendix A. Supplementary material

Scheme of multilayer growth, Deconvoluted XPS spectrum, Voltammetry (ECSA) and comparative table of catalysts. Supplementary data associated with this article can be found, in the online version, at https://doi.org/10.1016/j.apsusc.2018.03.235.

## References

[1] A. Kudo, Y. Miseki, Heterogeneous photocatalyst materials for water splitting, Chem. Soc. Rev. 38 (2009) 253–278, https://doi.org/10.1039/B800489G.
[2] C. Zhang, M. Shao, L. Zhou, Z. Li, K. Xiao, M. Wei, Hierarchical NiFe layered double hydroxide hollow microspheres with highly-efficient behavior toward oxygen evolution reaction (acsami.6b12100) ACS Appl. Mater. Interfaces (2016), https://doi.org/10.1021/acsami.6b12100.
[3] J.W.D. Ng, M. Tang, T.F. Jaramillo, A carbon-free, precious-metal-free, high-performance $O_2$ electrode for regenerative fuel cells and metal–air batteries, Energy Environ. Sci. 7 (2014) 2017, https://doi.org/10.1039/c3ee44059a.
[4] T.R. Cook, D.K. Dogutan, S.Y. Reece, Y. Surendranath, T.S. Teets, D.G. Nocera, Solar energy supply and storage for the legacy and non legacy worlds, Chem. Rev. 110 (2010) 6474–6502, https://doi.org/10.1021/cr100246c.
[5] D.D. Papadias, S. Ahmed, R. Kumar, F. Joseck, Hydrogen quality for fuel cell vehicles - A modeling study of the sensitivity of impurity content in hydrogen to the process variables in the SMR-PSA pathway, Int. J. Hydrogen Energy. 34 (2009) 6021–6035, https://doi.org/10.1016/j.ijhydene.2009.06.026.
[6] A. Haryanto, S. Fernando, N. Murali, S. Adhikari, Current status of hydrogen production techniques by steam reforming of ethanol: a review, Energy Fuels 19 (2005) 2098–2106, https://doi.org/10.1021/ef0500538.
[7] S. Kim, M. Cho, Y. Lee, Iridium oxide dendrite as a highly efficient dual electrocatalyst for water splitting and sensing of $H_2O_2$, J. Electrochem. Soc. 164 (2017) B3029–B3035, https://doi.org/10.1149/2.0061705jes.
[8] R. Forgie, G. Bugosh, K.C. Neyerlin, Z. Liu, P. Strasser, Bimetallic Ru electrocatalysts for the OER and electrolytic water splitting in acidic media, Electrochem. Solid-State Lett. 13 (2010) B36, https://doi.org/10.1149/1.3290735.

[9] C.C.L. McCrory, S. Jung, J.C. Peters, T.F. Jaramillo, Benchmarking heterogeneous electrocatalysts for the oxygen evolution reaction, J. Am. Chem. Soc. 135 (2013) 16977–16987, https://doi.org/10.1021/ja407115p.

[10] J. Qi, W. Zhang, R. Xiang, K. Liu, H. Wang, M. Chen, Porous nickel – iron oxide as a highly efficient electrocatalyst for oxygen evolution reaction, Adv. Sci. 2 (2015) 1500199, https://doi.org/10.1002/advs.201500199.

[11] L. Zhuang, L. Ge, Y. Yang, M. Li, Y. Jia, X. Yao, Z. Zhu, Ultrathin iron-cobalt oxide nanosheets with abundant oxygen vacancies for the oxygen evolution reaction, Adv. Mater. (2017) 1606793, https://doi.org/10.1002/adma.201606793.

[12] D.H. Youn, Y. Bin Park, J.Y. Kim, G. Magesh, Y.J. Jang, J.S. Lee, One-pot synthesis of NiFe layered double hydroxide/reduced graphene oxide composite as an efficient electrocatalyst for electrochemical and photoelectrochemical water oxidation, J. Power Sources 294 (2015) 437–443, https://doi.org/10.1016/j.jpowsour.2015.06.098.

[13] K. Fominykh, P. Chernev, I. Zaharieva, J. Sicklinger, G. Stefanic, M. Döblinger, A. Müller, A. Pokharel, S. Böcklein, C. Scheu, T. Bein, D. Fattakhova-Rohlfing, Iron-doped nickel oxide nanocrystals as highly efficient electrocatalysts for alkaline water splitting, ACS Nano 9 (2015) 5180–5188, https://doi.org/10.1021/acsnano.5b00520.

[14] M. Gong, Y. Li, H. Wang, Y. Liang, J.Z. Wu, J. Zhou, J. Wang, T. Regier, F. Wei, H. Dai, An advanced Ni-Fe layered double hydroxide electrocatalyst for water oxidation, J. Am. Chem. Soc. 135 (2013) 8452–8455, https://doi.org/10.1021/ja4027715.

[15] J. Chi, H. Yu, B. Qin, L. Fu, J. Jia, B. Yi, Z. Shao, Vertically aligned FeOOH/NiFe layered double hydroxides electrode for highly efficient oxygen evolution reaction, ACS Appl. Mater. Interfaces 9 (2017) 464–471, https://doi.org/10.1021/acsami.6b13360.

[16] Q. Liu, H. Wang, X. Wang, R. Tong, X. Zhou, X. Peng, H. Wang, H. Tao, Z. Zhang, Bifunctional $Ni_{1-x}Fe_x$ layered double hydroxides/Ni foam electrodes for high-efficient overall water splitting: a study on compositional tuning and valence state evolution, Int. J. Hydrogen Energy (2016) 1–9, https://doi.org/10.1016/j.ijhydene.2016.06.056.

[17] E. Nurlaela, T. Shinagawa, M. Qureshi, D.S. Dhawale, K. Takanabe, Temperature dependence of electrocatalytic and photocatalytic oxygen evolution reaction rates using NiFe oxide, ACS Catal. 6 (2016) 1713–1722, https://doi.org/10.1021/acscatal.5b02804.

[18] A.M.P. Sakita, R. Della Noce, E. Vallés, A.V. Benedetti, Pulse electrodeposition of CoFe thin films covered with layered double hydroxides as a fast route to prepare enhanced catalysts for oxygen evolution reaction, Appl. Surf. Sci. 434 (2018) 1153–1160, https://doi.org/10.1016/j.apsusc.2017.11.042.

[19] L.-K. Wu, J.-M. Hu, A silica co-electrodeposition route to nanoporous Co3O4 film electrode for oxygen evolution reaction, Electrochim. Acta. 116 (2014) 158–163, https://doi.org/10.1016/j.electacta.2013.11.010.

[20] A.T. Swesi, J. Masud, M. Nath, Nickel selenide as a high-efficiency catalyst for oxygen evolution reaction, Energy Environ. Sci. 9 (2016), https://doi.org/10.1039/C5EE02463C.

[21] Y.-C. Liu, J.A. Koza, J.A. Switzer, Conversion of electrodeposited $Co(OH)_2$ to CoOOH and $Co_3O_4$, and comparison of their catalytic activity for the oxygen evolution reaction, Electrochim. Acta 140 (2014) 359–365, https://doi.org/10.1016/j.electacta.2014.04.036.

[22] B. Dong, X. Zhao, G.-Q. Han, X. Li, X. Shang, Y.-R. Liu, W.-H. Hu, Y.-M. Chai, H. Zhao, C.-G. Liu, Two-step synthesis of binary Ni–Fe sulfides supported on nickel foam as highly efficient electrocatalysts for the oxygen evolution reaction, J. Mater. Chem. A (2016), https://doi.org/10.1039/C6TA03177C.

[23] Y. Sun, C. Liu, L. Zhang, P. Wan, S. Zhuang, Y. Tang, Y. Chen, J. Pan, Ultrafast electrodeposition of Ni−Fe hydroxide nanosheets on nickel foam as oxygen evolution anode for energy-saving electrolysis of $Na_2CO_3$/$NaHCO_3$, ChemElectroChem 4 (2017) 1044–1050, https://doi.org/10.1002/celc.201600713.

[24] P.T. Babar, A.C. Lokhande, B.S. Pawar, M.G. Gang, E. Jo, C. Go, M.P. Suryawanshi, S.M. Pawar, J.H. Kim, Electrocatalytic performance evaluation of cobalt hydroxide and cobalt oxide thin films for oxygen evolution reaction, Appl. Surf. Sci. 427 (2018) 253–259, https://doi.org/10.1016/j.apsusc.2017.07.142.

[25] K.H. Kim, J.Y. Zheng, W. Shin, Y.S. Kang, Preparation of dendritic NiFe films by electrodeposition for oxygen evolution, RSC Adv. 2 (2012) 4759, https://doi.org/10.1039/c2ra20241g.

[26] Y. Ullal, A.C. Hegde, Electrodeposition and electro-catalytic study of nanocrystalline Ni-Fe alloy, Int. J. Hydrogen Energy 39 (2014) 10485–10492, https://doi.org/10.1016/j.ijhydene.2014.05.016.

[27] W.G. Proud, C. Müller, The electrodeposition of nickel on vitreous carbon: Impedance studies, Electrochim. Acta. 38 (1993) 405–413, https://doi.org/10.1016/0013-4686(93)85158-U.

[28] J. Ji, W.C. Cooper, D.B. Dreisinger, E. Peters, Surface pH measurements during nickel electrodeposition, J. Appl. Electrochem. 25 (1995) 642–650, https://doi.org/10.1007/BF00241925.

[29] E. Gómez, R. Pollina, E. Vallés, Nickel electrodeposition on different metallic substrates, J. Electroanal. Chem. 386 (1995) 45–56, https://doi.org/10.1016/0022-0728(95)03817-Z.

[30] X. Tian, Y. Liu, D. Xiao, J. Sun, Ultrafast and large scale preparation of superior catalyst for oxygen evolution reaction, J. Power Sources 365 (2017) 320–326, https://doi.org/10.1016/j.jpowsour.2017.08.099.

[31] Y. Li, M. Zhao, Y. Zhao, L. Song, Z. Zhang, FeNi layered double-hydroxide nanosheets on a 3D carbon network as an efficient electrocatalyst for the oxygen evolution reaction, Part. Part. Syst. Charact. 33 (2016) 158–166, https://doi.org/10.1002/ppsc.201500228.

[32] A. Kargar, S. Yavuz, T.K. Kim, C.H. Liu, C. Kuru, C.S. Rustomji, S. Jin, P.R. Bandaru, Solution-processed $CoFe_2O_4$ nanoparticles on 3D carbon fiber papers for durable oxygen evolution reaction, ACS Appl. Mater. Interfaces 7 (2015) 17851–17856, https://doi.org/10.1021/acsami.5b04270.

[33] R. Oriňáková, M. Strečková, L. Trnkova, R. Rozik, M. Galova, Comparison of chloride and sulphate electrolytes in nickel electrodeposition on a paraffin impregnated graphite electrode, J. Electroanal. Chem. 594 (2006) 152–159, https://doi.org/10.1016/j.jelechem.2006.05.031.

[34] R. Wang, U. Bertocci, H. Tan, L.A. Bendersky, T.P. Moffat, Self-terminated electrodeposition of Ni Co, and Fe ultrathin films, J. Phys. Chem. C. 120 (2016) 16228–16237, https://doi.org/10.1021/acs.jpcc.6b01901.

[35] K. Yin, B. Lin, Effects of boric acid on the electrodeposition of iron, nickel and iron-nickel, Surf. Coat. Technol. 78 (1996) (accessed August 25, 2014) http://www.sciencedirect.com/science/article/pii/0257897294024103.

[36] I. Puigdomenech, Medusa, 2015, <https://www.kth.se/en/che/medusa>.

[37] W. Shao, G. Zangari, Dendritic growth and morphology selection in copper electrodeposition from acidic sulfate solutions containing chlorides, J. Phys. Chem. C. 113 (2009) 10097–10102, https://doi.org/10.1021/jp8095456.

[38] R. Oriňáková, A. Turoňová, D. Kladeková, M. Gálová, R.M. Smith, Recent developments in the electrodeposition of nickel and some nickel-based alloys, J. Appl. Electrochem. 36 (2006) 957–972, https://doi.org/10.1007/s10800-006-9162-7.

[39] N.L. Ritzert, T.P. Moffat, Ultramicroelectrode studies of self-terminated nickel electrodeposition and nickel hydroxide formation upon water reduction, J. Phys. Chem. C. 120 (2016) 27478–27489, https://doi.org/10.1021/acs.jpcc.6b10006.

[40] S.S. Djokić, M.D. Maksimović, Electrodeposition of Nickel-iron Alloys, 1992, pp. 417–466, 10.1007/978-1-4615-3376-4_4.

[41] A.P. Grosvenor, M.C. Biesinger, R.S.C. Smart, N.S. McIntyre, New interpretations of XPS spectra of nickel metal and oxides, Surf. Sci. 600 (2006) 1771–1779, https://doi.org/10.1016/j.susc.2006.01.041.

[42] Y.Q. Gao, X.Y. Liu, G.W. Yang, Amorphous mixed-metal hydroxide nanostructures for advanced water oxidation catalysts, Nanoscale. 8 (2016) 5015–5023, https://doi.org/10.1039/c5nr08989a.

[43] Y. Mu, F. Jia, Z. Ai, L. Zhang, Iron oxide shell mediated environmental remediation properties of nano zero-valent iron, Environ. Sci. Nano. 4 (2017) 27–45, https://doi.org/10.1039/C6EN00398B.

[44] X. Li, X. Hao, Z. Wang, A. Abudula, G. Guan, In-situ intercalation of NiFe LDH materials: an efficient approach to improve electrocatalytic activity and stability for water splitting, J. Power Sources. 347 (2017) 193–200, https://doi.org/10.1016/j.jpowsour.2017.02.062.

[45] N. Mahmood, M. Tahir, A. Mahmood, J. Zhu, C. Cao, Y. Hou, Chlorine-doped carbonated cobalt hydroxide for supercapacitors with enormously high pseudocapacitive performance and energy density, Nano Energy 11 (2015) 267–276, https://doi.org/10.1016/j.nanoen.2014.11.015.

[46] V.M. Jiménez, A. Fernández, J.P. Espinós, A.R. González-Elipe, The state of the oxygen at the surface of polycrystalline cobalt oxide, J. Electron Spectros. Relat. Phenom. 71 (1995) 61–71, https://doi.org/10.1016/0368-2048(94)02238-0.

[47] X.-F. Lu, D.-J. Wu, R.-Z. Li, Q. Li, S.-H. Ye, Y.-X. Tong, G.-R. Li, Hierarchical $NiCo_2O_4$ nanosheets@hollow microrod arrays for high-performance asymmetric supercapacitors, J. Mater. Chem. A. 2 (2014) 4706–4713, https://doi.org/10.1039/C3TA14930G.

[48] W. Chang, Y. Wei, J. Guo, F. He, Thermal stability of Ni-Fe alloy foils continuously electrodeposited in a fluorborate bath, Open J. Met. 2012 (2012) 18–23, https://doi.org/10.4236/ojmetal.2012.21003.

[49] A. Djekoun, B. Bouzabata, A. Otmani, J.M. Greneche, X-ray diffraction and Mössbauer studies of nanocrystalline Fe-Ni alloys prepared by mechanical alloying, Catal. Today 89 (2004) 319–323, https://doi.org/10.1016/j.cattod.2003.12.018.

[50] D.L. Grimmett, A comparison of DC and pulsed Fe-Ni alloy deposits, J. Electrochem. Soc. 140 (1993) 973, https://doi.org/10.1149/1.2056238.

[51] B.M. Hunter, W. Hieringer, J.R. Winkler, H.B. Gray, A.M. Müller, Effect of interlayer anions on [NiFe]-LDH nanosheet water oxidation activity, Energy Environ. Sci. 9 (2016) 1734–1743, https://doi.org/10.1039/C6EE00377J.

[52] L. Trotochaud, S.L. Young, J.K. Ranney, S.W. Boettcher, Nickel-Iron oxyhydroxide oxygen-evolution electrocatalysts: the role of intentional and incidental iron incorporation, J. Am. Chem. Soc. 136 (2014) 6744–6753, https://doi.org/10.1021/ja502379c.

[53] M.W. Louie, A.T. Bell, An investigation of thin-film Ni-Fe oxide catalysts for the electrochemical evolution of oxygen, J. Am. Chem. Soc. 135 (2013) 12329–12337, https://doi.org/10.1021/ja405351s.

[54] R.L. Doyle, I.J. Godwin, M.P. Brandon, M.E. Lyons, Redox and electrochemical water splitting catalytic properties of hydrated metal oxide modified electrodes, Phys. Chem. Chem. Phys. 15 (2013) 13737–13783, https://doi.org/10.1039/c3cp51213d.

[55] Y. Kou, J. Liu, Y. Li, S. Qu, C. Ma, Z. Song, X. Han, Y. Deng, W. Hu, C. Zhong, Electrochemical oxidation of chlorine-doped Co(OH)2 nanosheet arrays on carbon cloth as a bifunctional oxygen electrode, ACS Appl. Mater. Interfaces (2017), https://doi.org/10.1021/acsami.7b17002 (acsami.7b17002).

[56] D. Friebel, M.W. Louie, M. Bajdich, K.E. Sanwald, Y. Cai, A.M. Wise, M.J. Cheng, D. Sokaras, T.C. Weng, R. Alonso-Mori, R.C. Davis, J.R. Bargar, J.K. Nørskov, A. Nilsson, A.T. Bell, Identification of highly active Fe sites in (Ni, Fe)OOH for

electrocatalytic water splitting, J. Am. Chem. Soc. 137 (2015) 1305–1313, https://doi.org/10.1021/ja511559d.
[57] M.B. Stevens, C.D.M. Trang, L.J. Enman, J. Deng, S.W. Boettcher, Reactive Fe-sites in Ni/Fe (Oxy)hydroxide are responsible for exceptional oxygen electrocatalysis activity, J. Am. Chem. Soc. 139 (2017) 11361–11364, https://doi.org/10.1021/jacs.7b07117.
[58] S. Klaus, Y. Cai, M.W. Louie, L. Trotochaud, A.T. Bell, Effects of Fe electrolyte impurities on $Ni(OH)_2$/NiOOH structure and oxygen evolution activity, J. Phys. Chem. C. 119 (2015) 7243–7254, https://doi.org/10.1021/acs.jpcc.5b00105.
[59] S. Klaus, M.W. Louie, L. Trotochaud, A.T. Bell, Role of catalyst preparation on the electrocatalytic activity of $Ni_{1-x}Fe_xOOH$ for the oxygen evolution reaction, J. Phys. Chem. C. 119 (2015) 18303–18316, https://doi.org/10.1021/acs.jpcc.5b04776.